# Mathematical Model of Novel Wound-Field Synchronous Motor Self-Excited by Space Harmonics

Masahiro Aoyama/Shizuoka University, Suzuki Motor Corporation
Department of Environment and Energy System, Graduate School of Science and Technology
3-5-1 Johoku, Naka-Ku, Hamamatsu, Shizuoka 432-8561, Japan
aoyamam@hhq.suzuki.co.jp

Toshihiko Noguchi/Shizuoka University
Department of Electrical and Electric Engineering, Graduate School of Engineering
3-5-1 Johoku, Naka-Ku, Hamamatsu, Shizuoka 432-8561, Japan
ttnogut@ipc.shizuoka.ac.jp

***Abstract*—This paper describes mathematical modeling of a novel wound-field synchronous motor self-excited by space harmonics. The torque equation on the *dq*-reference frame is investigated to clarify the self-excitation mechanism of the proposed motor. It has been analytically explicated how the motor parameters give influences on the self-excited electromagnet torque. Furthermore, the current phase vs. torque characteristics are compared between the FEM based simulation result and the mathematical calculation result. Both of the results showed good agreement, which proves feasibility of the mathematical modeling discussed in the paper.**

***Keywords*— mathematical model; synchronous motor; self-excitation; space harmonics; concentrated winding.**

## I. INTRODUCTION

Internal combustion engine based automotive vehicles can be more efficient by introducing electric components such as motors and generators to their drive trains. The advancement of the drive train performance contributes to mitigate the global warming through reduction of CO2 emission and fuel consumption. Even a simple improvement such as an idling-stop system, which is an entry level system of the vehicle electrification, has a remarkable impact on the total efficiency of the vehicles. As the degree of electrification is higher, more advantages can be expected whereas the system becomes more complicated. An electric machine is one of the key components in hybrid vehicles (HEVs) and electric vehicles (EVs) from the viewpoint of dynamic and fuel consumption performances. Traction motors for the HEVs require a wide adjustable speed drive range, high maximum torque, and high power density without sacrificing its power conversion efficiency. Particularly, an IPM (Interior Permanent Magnet) motor is often applied to the HEVs owing to its highly improved efficiency and specific power per physical volume. Permanent magnets used for the IPM motor are relatively expensive because Nd-Fe-B magnets are generally employed to realize high energy density and to improve fuel efficiency in the low-load operation for street use. Moreover, more expensive rare-earth metals such as Dy and Tb must be added to the Nd-Fe-B magnet to restrain demagnetization caused by the high temperate.

Therefore, varieties of rare-earth-free motors, particularly wound-field synchronous motor which replaces magnets with electromagnets, are focused due to remarkable rise of the Nd-Fe-B magnet market price [1][2]. For example, a separate excitation wound-field synchronous motor is proposed in [2]. This motor is capable to utilize the armature reaction torque by the wound-field torque, and the field magnetization control allows high efficiency operation. An external chopper circuit is, however, indispensable for the wound-field winding. Furthermore, it is rather difficult to transfer the field magnetization power from the primary to the secondary of the motor, and an extra copper loss in the wound-field winding is also a serious problem. Thus, a brushless-excitation technique proposed in [3] is reevaluated by the authors to solve the problems regarding the separate excitation wound-field motors. This classic brushless-excitation based synchronous motor has a stator with distributed windings (3 phase-4 poles) and a salient pole rotor (4 poles) with a single winding connected via a half-bridge rectifier. The harmonic components of an armature magnetomotive force are generated by 2-pole direct current excitation windings, and link to the rotor winding for the field magnetization. Another classic brushless-excitation technique, which has rotor windings with a diode rectifier, is proposed in [4]. This self-excitation technique utilizes the inverted magnetic field generated by auxiliary armature capacitor winding for the rotor magnetization, but the armature copper loss increases because the winding space factor detrimentally decreases.

This paper tries to solve the above problems of the classical wound-field synchronous motor, and proposes a novel configuration and operation mechanism of the self-excitation, focusing on the space harmonics power. Particularly, a mathematical model of the proposed motor

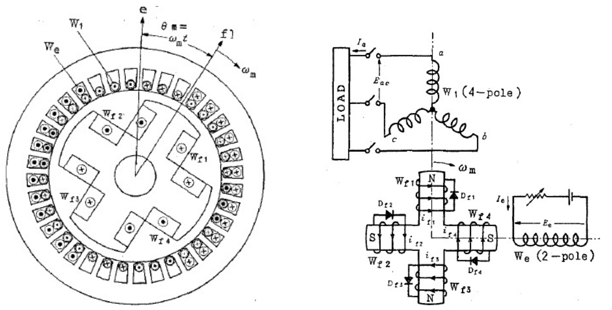

(a) Cross section diagram. (b) Rotor and stator winding connection.
Fig. 1. Classic self-excitation synchronous motor.

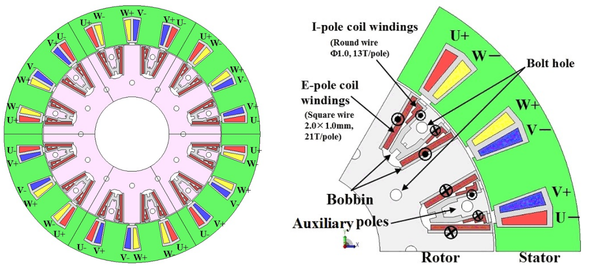


(a) Cross section diagram. (b) Detailed winding configuration.
Fig. 2. Proposed self-excitation synchronous motor.

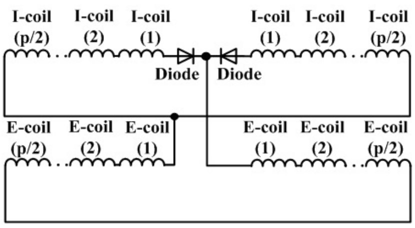


Fig. 3. Rotor winding connection of proposed motor.

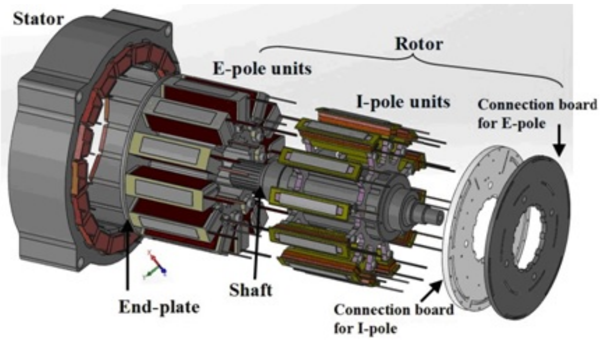


Fig. 4. Mechanical configuration of proposed motor.

is discussed in the paper for the purpose of designing a high-efficiency drive.

## II. Outline of Proposed Motor

Figure 1 shows a classic blushless-excitation synchronous motor presented in [3]. The motor has a direct current winding connected to an external chopper circuit in the stator slots in addition to the three-phase armature windings for excitation. The direct current winding is indispensable to acquire the second harmonic component for the excitation because the three-phase distributed windings generate only the rotating magnetic field. The proposed motor has, however, concentrated armature windings not to use any special excitation windings in the stator. Conventional common motors dissipate space harmonics power caused by the concentrated stator and the salient pole configuration, whereas the proposed motor positively utilizes the space harmonics power for the excitation. Figure 2 shows the proposed self-excitation motor where the wound-field windings are added to the rotor salient poles and the induction coils are placed in spaces between the rotor salient poles, i.e., rotor slots. Each of the induction poles (I-poles) is a special pole exclusively used to generate the magnetizing power from the third space harmonics. On the other hand, each excitation pole (E-pole) is a salient pole of the rotor magnetized by the I-poles, which uses the retrieved third space harmonics power. Every I-pole and E-pole is connected in series via a diode rectifying circuit as shown in Fig. 3, where p indicates a pole number. The I-pole is an auxiliary pole that induces a voltage proportional to the derivative of the third space harmonic flux, and is designed to be magnetically independent of the main magnetic path to prevent reduction of the saliency. Every I-pole is mechanically held from an axial direction using support ring boards as shown in Fig. 4. Specifications of the proposed motor shown in Fig. 2 are listed in Table I.

TABLE I. SPECIFICATIONS OF MOTOR.

| | |
|---|---|
| Number of poles | 12 |
| Number of slots | 18 |
| Stator outer diameter | 200 mm |
| Rotor diameter | 138.6 mm |
| Axial length of core | 54 mm |
| Air gap length | 0.7 mm |
| Maximum current | 273 $A_{pk}$ (45 s) |
| Stator winding resistance | 32.1 mΩ / phase |
| Number of coil-turn | 48 |
| Winding connection | 6 parallel |
| I-pole winding resistance | 37.0 mΩ / pole |
| E-pole winding resistance | 28.2 mΩ / pole |
| Thickness of iron core steel plate | 0.35 mm |

## III. Theoretical Analysis of Proposed Motor

### *A. Principle of Third Space Harmonics Generation*

The proposed motor can obtain the field magnetization power from the third space harmonics owing to the slot combination between the rotor pole counts and the stator slot counts. Figure 5 shows the magnetic flux density, the flux lines and the *d*-axis inductance variation of the 2pole-6slot motor. The *d*-axis inductance consists of a constant part and a sixth slot harmonics part periodically changes with the rotation. On the other hand, in the case of a fractional slot winding motor such as a 2pole-3slot one, the *d*-axis inductance variation is caused in a slightly different manner. As illustrated in Fig. 6, one of the rotor salient pole and the other are not always symmetric. If the

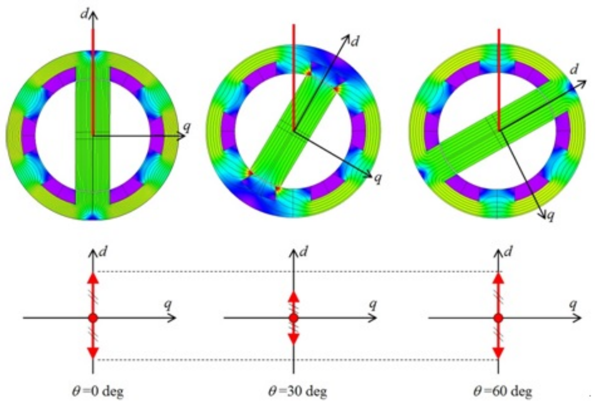


Fig. 5. *d*-axis inductance variation of 2pole-6slot motor.

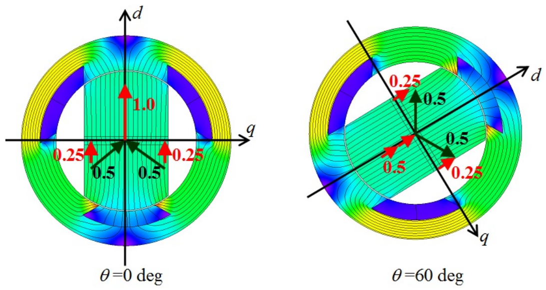


Fig. 6. *d*-axis inductance variation depending on rotor position.

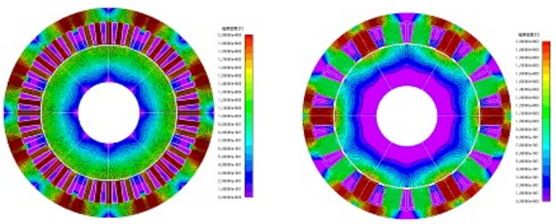

(a) Distributed windings. (b) Concentrated windings.

Fig. 7. Magnetic flux density and flux lines for solid rotor.

rotor position is $\theta$=0 deg, the positive direction of the *d*-axis coincides with one of the stator teeth, but the opposite salient pole of the *d*-axis faces with a slot. Therefore, the opposite pole forms a closed magnetic circuit with interference between the *d*-*q* axes. On the other hand, if the rotor position is $\theta$=30 deg, the positive direction of the *d*-axis is oriented to the slot, where the magnetic reluctance is relatively high. As described above, the 2pole-3slot motor has a *d*-axis inductance composed with a constant part and a periodical third space harmonics part according to the rotation. This periodical variation of the inductance is particularly caused by the doubly salient configuration of the motor. Figure 7 shows magnetic flux density distributions of the distributed winding and the concentrated winding configurations when a bulk solid rotor is used. Figure 8 shows magnetic flux waveforms linking to the armature windings for both winding configurations. As can be seen in the figures, the armature magnetic fluxes of the distributed winding configuration are sinusoidal waveforms, but the fluxes of the concentrated one are close to trapezoidal waveforms, which mainly include the fifth and seventh space harmonics. Figure 9 shows *d*-axis inductance variation with respect to the electrical angle of a 2pole-3slot concentrated winding and an 8pole-48slot distributed winding configurations. As shown in the figure, the periodical variation of the *d*-axis inductance caused by the

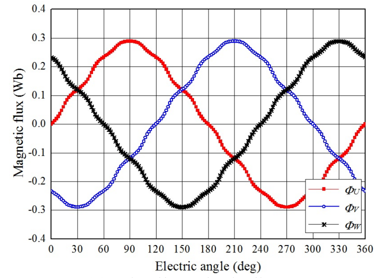


(a) Distributed windings.

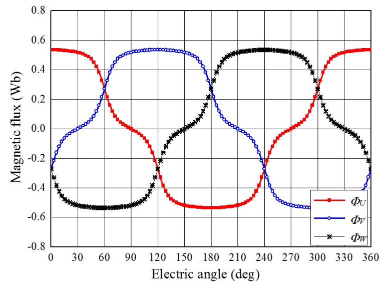


(b) Concentrated windings.

Fig. 8. Magnetic flux waveform linking to armature winding.

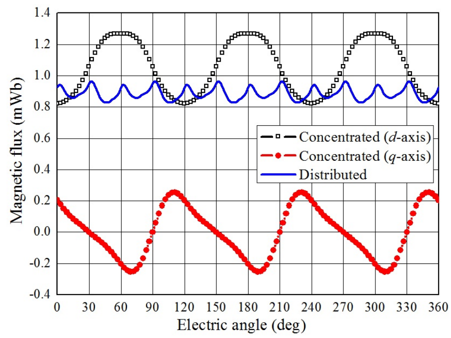


Fig. 9. *d*-axis inductance variation of 2pole-3slot concentrated winding and 8pole-48slot distributed winding configurations.

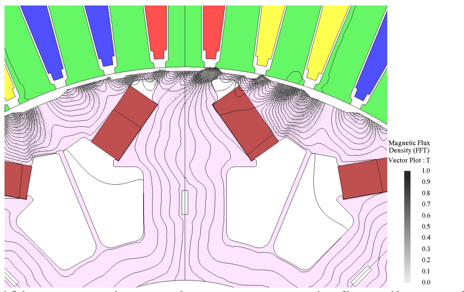


(a) Twelfth space harmonics vector and flux lines of distributed winding configuration.

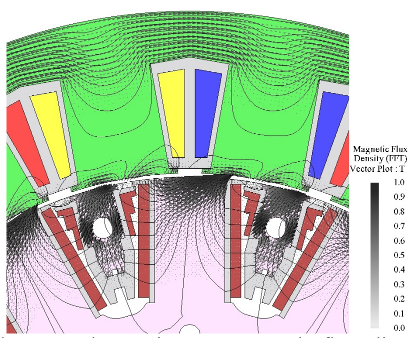


(b) Third space harmonics vector and flux lines of concentrated winding configuration.

Fig. 10. Comparison of space harmonics vector and flux lines.

slot harmonics is observed on the constant DC components, and the third space harmonic component of the concentrated winding configuration is much larger than the ripples of the distributed one. Figure 10 shows the main space harmonics vector and flux lines of the two winding configurations. It is found that the third space harmonic flux, which is caused by the 2 to 3 slot combination, links deeply into the rotor although the twelfth space harmonic flux generated by the distributed winding configuration links around the rotor surface. In addition, the third space harmonic flux goes mainly through the rotor salient pole and the slot. This is the reason why the I-pole must be placed on the $q$-axis, which is the most efficient way to retrieve the third space harmonic power.

### *B. Mathematical Model on dq-Reference Frame*

The operation principle of the proposed motor can be explicated by voltage equations on the synchronous rotating reference frame. As shown in Fig. 9, the $d$-axis inductance $L_d$ and the $q$-axis inductance $L_q$ can be given by

$$L_d(\omega t) = L_{d0} + L_{da}\cos 3\omega t \text{, and} \tag{1}$$

$$L_q(\omega t) = L_{q0} + L_{qa}\sin\left(-3\left(\omega t - \frac{\pi}{6}\right)\right) = L_{q0} + L_{qa}\sin 3\omega t \text{,} \tag{2}$$

where $L_{d0}$ and $L_{q0}$ are constant parts, and $L_{da}$ and $L_{qa}$ are amplitudes of the periodical variations. $\omega$ is an electrical synchronous angular velocity. The mathematical model of the proposed motor can be expressed as the following voltage equation:

$$\begin{bmatrix} v_{sd} \\ v_{sq} \end{bmatrix} = \begin{bmatrix} R_s & 0 \\ 0 & R_s \end{bmatrix}\begin{bmatrix} i_{sd} \\ i_{sq} \end{bmatrix} + \begin{bmatrix} \mathrm{p} & -\omega \\ \omega & \mathrm{p} \end{bmatrix}\begin{bmatrix} \psi_{sd} \\ \psi_{sq} \end{bmatrix}$$

$$= \begin{bmatrix} R_s & 0 \\ 0 & R_s \end{bmatrix}\begin{bmatrix} i_{sd} \\ i_{sq} \end{bmatrix} + \begin{bmatrix} \mathrm{p} & -\omega \\ \omega & \mathrm{p} \end{bmatrix}\begin{bmatrix} L_d & 0 & M_d & 0 \\ 0 & L_q & 0 & M_q \end{bmatrix}\begin{bmatrix} i_{sd} \\ i_{sq} \\ i_{rd} \\ i_{rq} \end{bmatrix}, \tag{3}$$

where $v_{sd}$, $v_{sq}$, $i_{sd}$ and $i_{sq}$ are armature voltages and currents, $i_{rd}$ and $i_{rq}$ are a $d$-axis and a $q$-axis rotor winding currents, $R_s$ is an armature winding resistance, $M_d$ and $M_q$ are a $d$-axis and a $q$-axis mutual inductances, p denotes a differential operator, respectively. The self inductances on the $dq$-reference frame vary periodically with respect to the time as expressed by Eqs. (1) and (2). Hence, Eq. (3) can be rewritten as follows:

$$\begin{aligned} \begin{bmatrix} v_{sd} \\ v_{sq} \end{bmatrix} &= \begin{bmatrix} R_s & 0 \\ 0 & R_s \end{bmatrix}\begin{bmatrix} i_{sd} \\ i_{sq} \end{bmatrix} + \begin{bmatrix} L_d & 0 & M_d & 0 \\ 0 & L_q & 0 & M_q \end{bmatrix}\mathrm{p}\begin{bmatrix} i_{sd} \\ i_{sq} \\ i_{rd} \\ i_{rq} \end{bmatrix} \\ &+ \begin{bmatrix} \mathrm{p}L_d & 0 & \mathrm{p}M_d & 0 \\ 0 & \mathrm{p}L_q & 0 & \mathrm{p}M_q \end{bmatrix}\begin{bmatrix} i_{sd} \\ i_{sq} \\ i_{rd} \\ i_{rq} \end{bmatrix} \\ &+ \omega\begin{bmatrix} 0 & -L_q & 0 & -M_q \\ L_d & 0 & M_d & 0 \end{bmatrix}\begin{bmatrix} i_{sd} \\ i_{sq} \\ i_{rd} \\ i_{rq} \end{bmatrix} \end{aligned} \quad . \tag{4}$$

In the above voltage equation, the mutual inductance $M_d$ and $M_q$ can be simply expressed as follows by using the number of turns of the $d$-axis, $q$-axis rotor windings and the stator windings $N_{rd}$, $N_{rq}$ and $N_S$:

$$M_d = \frac{N_{rd}}{N_S}K_{Ld}L_d = \frac{N_{rd}}{N_S}K_{Ld}\left(L_{d0} + L_{da}\cos 3\omega t\right)\text{, and} \tag{5}$$

$$M_q = \frac{N_{rd}}{N_S}K_{Lq}L_q = \frac{N_{rq}}{N_S}K_{Ld}\left(L_{q0} + L_{qa}\sin 3\omega t\right)\text{,} \tag{6}$$

where $K_{Ld}$ and $K_{Lq}$ are leakage magnetic flux coefficients of the $d$-axis and $q$-axis. Substituting the time derivatives of $L_d$, $L_q$, $M_d$ and $M_q$ into the third term of Eq. (4), the mathematical model of the motor is expressed as

$$\begin{aligned} \begin{bmatrix} v_{sd} \\ v_{sq} \end{bmatrix} &= \begin{bmatrix} R_s & 0 \\ 0 & R_s \end{bmatrix}\begin{bmatrix} i_{sd} \\ i_{sq} \end{bmatrix} + \begin{bmatrix} L_d & 0 & \frac{N_{rd}}{N_S}K_{Ld}L_d & 0 \\ 0 & L_q & 0 & \frac{N_{rq}}{N_S}K_{Lq}L_q \end{bmatrix}\mathrm{p}\begin{bmatrix} i_{sd} \\ i_{sq} \\ i_{rd} \\ i_{rq} \end{bmatrix} \\ &+ \omega\begin{bmatrix} -3L_{da}\left(\frac{L_q - L_{q0}}{L_{qa}}\right) & -L_q & -\frac{N_{rd}}{N_S}K_{Ld}L_{da}\left(\frac{L_q - L_{q0}}{L_{qa}}\right) & -\frac{N_{rq}}{N_S}K_{Lq}L_q \\ L_d & 3L_{qa}\left(\frac{L_d - L_{d0}}{L_{da}}\right) & \frac{N_{rd}}{N_S}K_{Ld}L_d & \frac{N_{rq}}{N_S}K_{Lq}L_{qa}\left(\frac{L_d - L_{d0}}{L_{da}}\right) \end{bmatrix}\begin{bmatrix} i_{sd} \\ i_{sq} \\ i_{rd} \\ i_{rq} \end{bmatrix} \end{aligned} \quad . \tag{7}$$

The first term of the above equation is an armature winding resistance voltage drop, the second term is a transformer electromotive force, and the third term is an electromotive force.

### *C. Field Current*

The rotor current $i_{rd}$ and $i_{rq}$ are expressed by using $i_{sd}$ and $i_{sq}$ because the field current $i_{rd}$ and the induced current $i_{rq}$ are caused by the flux linkage from the stator. The induced voltage of the I-pole windings is applied to the E-pole windings for the self excitation through the full-bridge rectifier. Thus, the voltage applied to the E-pole windings is an absolute value of the I-pole winding voltage, and is expressed as Eq. (12), using Fourier series:

$$\begin{aligned} v_{rd} = \left|v_{rq}\right| &= a_0 + \sum_{n=1}^{\infty}\left(a_n \cos n\left(\frac{2\pi}{\frac{T}{2}}\right)t + b_n \sin n\left(\frac{2\pi}{\frac{T}{2}}\right)t\right) \\ &= a_0 + \sum_{n=1}^{\infty}\left(a_n \cos 6n\omega t + b_n \sin 6n\omega t\right) \end{aligned}, \tag{8}$$

where $a_0$, $a_n$ and $b_n$ are Fourier series coefficients. In order to derive the I-pole winding voltage $v_{rq}$, the following magnetic fluxes on the $dq$-reference frame are considered:

$$\phi_d = L_d i_{sd} = \left(L_{d0} + L_{da}\cos 3\omega t\right)i_{sd}\text{, and} \tag{9}$$

$$\phi_q = L_q i_{sq} = \left(L_{q0} + L_{qa}\sin 3\omega t\right)i_{sq}\text{.} \tag{10}$$

By using the above equations, $v_{rq}$ can be calculated as

$$\begin{aligned} v_{rq} &= -N_{rq}\mathrm{p}\left(K_{d-axis}\phi_d + \phi_q\right) \\ &= -3\omega N_{rq}\left(-K_{d-axis}L_{da}i_{sd}\sin 3\omega t + L_{qa}i_{sq}\cos 3\omega t\right) \end{aligned}, \tag{11}$$

where $K_{d\text{-}axis}$ is a coefficient expressing interference between the two axes. This coefficient must be determined by the degree of the magnetic interference from the $d$-axis space harmonic flux onto the I-pole windings. By substituting the above expression into Eq. (8), the voltage applied to the E-pole windings $v_{rd}$ is obtained as follows:

$$v_{rd}=\frac{6\omega}{\pi}\begin{pmatrix} N_{rq}K_{d-axis}L_{da}i_{sd}\left(\frac{1}{2}+\sum_{n=1}^{\infty}\frac{1}{1-4n^2}\cos 6n\omega t\right) \\ +N_{rq}L_{qa}i_{sq}\left(\frac{1}{2}+\sum_{n=1}^{\infty}\frac{1}{1-4n^2}\cos 6n\omega t\right)\end{pmatrix}. \quad (12)$$

The DC component of $v_{rd}$ extracted from Eq. (12) can be given by

$$v_{rd(DC)}=\frac{3\omega N_{rq}}{\pi}\left(K_{d-axis}L_{da}i_{sd}+L_{qa}i_{sq}\right). \quad (13)$$

Since the DC voltage applied to the E-pole windings is a source of the field current $i_{rd}$, solving the transient response of the rotor winding gives the field current as expressed by the following equation:

$$i_{rd}(t)=\frac{3\omega N_{rq}}{\pi\left(R_{rd}+R_{rq}\right)}\left(K_{d-axis}L_{da}i_d+L_{qa}i_q\right)\left(1-e^{\frac{-\left(R_{rd}+R_{rq}\right)}{L_{rd}}t}\right). \quad (14)$$

## *D. Torque*

The motor model on the $dq$-reference frame can be further rewritten as follows, taking the above discussion into account:

$$\begin{aligned}\begin{bmatrix}v_d\\ v_q\end{bmatrix}&=\begin{bmatrix}R_s & 0\\ 0 & R_s\end{bmatrix}\begin{bmatrix}i_d\\ i_q\end{bmatrix}\\ &+\begin{bmatrix}L_d+3\omega K_{d-axis}L_{da}K_{Ld}L_dN_{rd} & 3\omega L_{qa}K_E\\ 3\omega K_{d-axis}L_{da}K_{Lq}L_q\frac{N_{rq}}{\pi}K_E & L_q+\frac{3\omega}{\pi}L_{qa}K_E\end{bmatrix}\mathrm{p}\begin{bmatrix}i_d\\ i_q\end{bmatrix},\\ &+\omega\begin{bmatrix}-3\left(L_{da}L_{qq}+\omega K_EK_{d-axis}L_{da}\left(N_{rd}K_{Ld}L_{da}L_{qq}+\frac{N_{rq}}{\pi}K_{Lq}L_q\right)\right) & * \\ L_d+3\omega K_EK_{d-axis}L_{da}\left(N_{rd}K_{Ld}L_d+\frac{N_{rq}}{\pi}K_{Lq}L_{qa}L_{dd}\right) & \end{bmatrix}\\ &\quad * \begin{bmatrix}-\left(L_q+3K_EK_{d-axis}L_{da}L_{qa}\left(N_{rd}K_{Ld}L_{da}L_{qq}+\frac{N_{rq}}{\pi}K_{Lq}L_q\right)\right)\\ 3\left(L_qL_{dd}+\omega K_EK_{d-axis}L_{da}L_{qa}\left(N_{rd}K_{Ld}L_d+\frac{N_{rq}}{\pi}K_{Lq}L_{qa}L_{dd}\right)\right)\end{bmatrix}\begin{bmatrix}i_d\\ i_q\end{bmatrix}\end{aligned} \quad (15)$$

where the coefficients $K_E$, $L_{dd}$ and $L_{qq}$ are given by Eqs. (20) and (21):

$$K_{E1}=\frac{N_{rq}}{\pi N_S\left(R_{rd}+R_{rq}\right)}, \quad (16)$$

$$L_{dd}=\frac{L_d-L_{d0}}{L_{da}}, \text{ and } L_{qq}=\frac{L_q-L_{q0}}{L_{qa}}. \quad (17)$$

The output torque of the proposed motor is obtained by the vector product between the armature current and the magnetic flux, which is described in a part of the third term of Eq. (7):

$$\begin{aligned}T&=P_p\begin{bmatrix}i_{sd} & i_{sq}\end{bmatrix}\begin{bmatrix}-3L_{da}L_{qq} & -L_q & * \\ L_d & 3L_{qa}L_{dd} & \end{bmatrix}\\ &\quad * \begin{bmatrix}-\frac{N_{rd}}{N_S}K_{Ld}L_{da}L_{qq} & -\frac{N_{rq}}{N_S}K_{Lq}L_q\\ \frac{N_{rd}}{N_S}K_{Ld}L_d & \frac{N_{rq}}{N_S}K_{Lq}L_{qa}L_{dd}\end{bmatrix}\begin{bmatrix}i_{sd}\\ i_{sq}\\ i_{rd}\\ i_{rq}\end{bmatrix}\\ &=P_p\left(L_d-L_q\right)i_{sd}i_{sq}+P_p\left(3\left(-L_{da}L_{qq}i_{sd}^2+L_{qa}L_{dd}i_{sq}^2\right)\right.\\ &\quad+\frac{N_{rd}}{N_S}K_{Ld}\left(-L_{da}L_{qq}i_{sd}+L_di_{sq}\right)i_{rd}\\ &\quad\left.+\frac{N_{rq}}{N_S}K_{Lq}\left(-L_qi_{sd}+L_{qa}L_{dd}i_{sq}\right)i_{rq}\right)\end{aligned}, \quad (18)$$

where $P_p$ is a pole-pair number. As expressed in the above expression, the output torque is composed of the two terms, i.e., reluctance torque and electromagnet torque. Therefore, output torque on the $dq$-reference frame at the steady-state can be obtained as:

$$\begin{aligned}T&=P_p\left(L_d-L_q\right)i_{sd}i_{sq}\\ &+P_p\begin{pmatrix}3\left(-L_{da}L_{qq}i_{sd}^2+L_{qa}L_{dd}i_{sq}^2\right)\\ +3\omega K_E\left(K_{d-axis}L_{da}i_d+L_{qa}i_q\right)\begin{pmatrix}N_{rd}K_{Ld}\left(-L_{da}L_{qa}i_d+L_di_q\right)\\ +\frac{N_{rq}}{\pi}K_{Lq}\left(-L_qi_d+L_qL_{dd}i_q\right)\end{pmatrix}\end{pmatrix}.\end{aligned} \quad (19)$$

Since the field current generating the electromagnet torque is proportional to $\omega$ as expressed by Eq. (14), the proposed motor cannot deliver the sufficient electromagnet torque in the low-speed range. In addition, because the electromagnet torque includes the leakage magnetic flux coefficients as shown in Eqs. (5) and (6) as well as the winding turn ratio between the stator and the rotor, their parameter values have significant impact on the torque generation.

# IV. VARIFICATION OF OPERATION CHARACTERISTICS

## *A. Current Phase vs. Torque Characteristics*

Figure 11 shows current phase vs. torque (average torque in the steady state) characteristics for 1000 r/min of the proposed motor calculated by FEM based computer simulations. The characteristics are calculated under the condition of use of a sinusoidal current source. Separation of the reluctance torque and the electromagnet torque is performed through the following steps:

1) calculation of the reluctance torque at the current phase of 45 deg without connecting the rotor windings,
2) determination of the current phase vs. reluctance torque characteristic by fitting a $\sin 2\beta$ trigonometric function of which amplitude is a torque value at 45 deg calculated in the previous step,
3) calculation of the current phase vs. total torque characteristic with the rotor windings connected, and
4) subtraction of the reluctance torque from the total torque to obtain the electromagnet torque separately.

As shown in Fig. 11, the electromagnet torque, i.e., an additional torque generated by the self-excitation using the space harmonics, is enlarged as the armature current becomes higher. Figure 12 shows the characteristics

TABLE II. INDUCTANCES USED FOR CALCULATION OF MATHEMATICAL MODEL.

| Inductance | $L_{d0}$ | | | $L_{q0}$ | | |
|---|---|---|---|---|---|---|
| Armature current | 100 $A_{pk}$ | 200 $A_{pk}$ | 273 $A_{pk}$ | 100 $A_{pk}$ | 200 $A_{pk}$ | 273 $A_{pk}$ |
| 500 r/min | - | - | 7.5 mH | - | - | 3.8 mH |
| 1000 r/min | 9.0 mH | 8.5 mH | 7.2 mH | 3.6 mH | 3.6 mH | 3.6 mH |
| 2000 r/min | - | - | 6.7 mH | - | - | 3.1 mH |
| 3000 r/min | - | - | 6.3 mH | - | - | 2.7 mH |

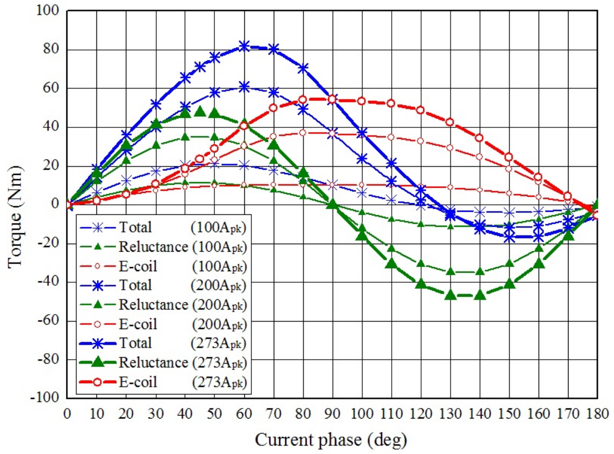


Fig. 11. Current phase vs. torque characteristics at 1000 r/min calculated by FEM model.

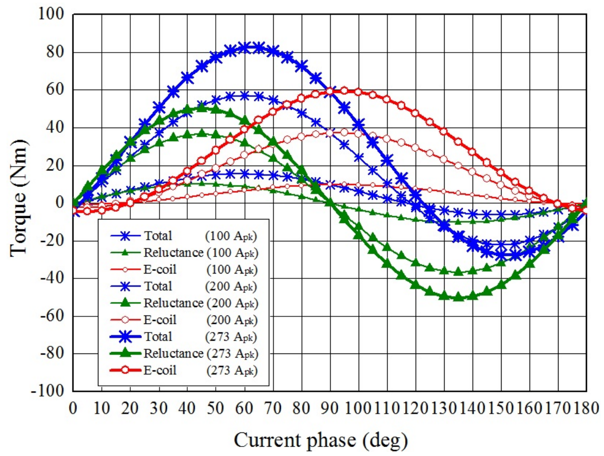


Fig. 12. Current phase vs. torque characteristics at 1000 r/min calculated by mathematical model.

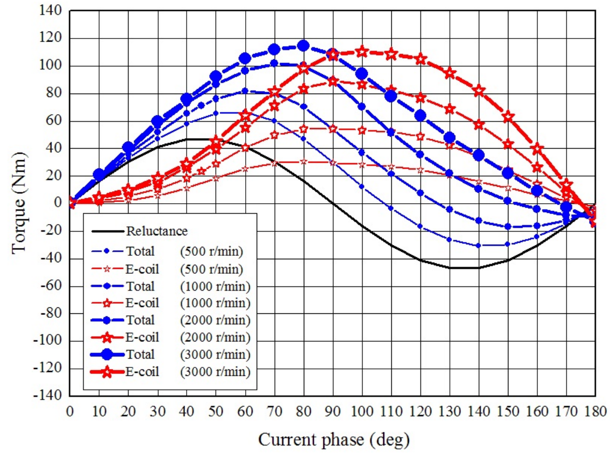


Fig. 13. Current phase vs. torque characteristics for 273 $A_{pk}$ calculated by FEM model.

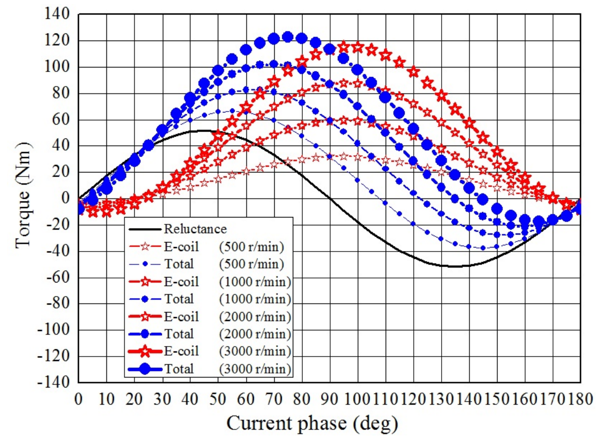


Fig. 14. Current phase vs. torque characteristics for 273 Apk calculated by mathematical model.

calculated by the mathematical model given by Eq. (19). The parameters used in Eq. (19) are listed in TABLES I and II, where the inductance variations caused by the magnetic saturation and the operating speed change are taken into account. The leakage magnetic flux coefficients used in the mathematical model are indicated in TABLE III. The periodical variations of the *d*-axis and the *q*-axis inductances are $L_{da}$=6.2×$10^{-3}$ mH and $L_{qa}$=8.8 ×$10^{-3}$ mH, respectively.

As can be seen in Figs. 11 and 12, both of the results have overall similar characteristics with indicating the same tendency. However, some errors of the electromagnet torque can be found in the region where the armature current phase is not advanced. The error must be caused by having ignored an interference that links from the *d*-axis space harmonics to the E-pole windings and by having ignored higher order space harmonics more than $2\omega$ (Approximated an ideal magnetomotive force distribution.)

## B. *Adjustable Speed Drive Characteristics*

Figures 13 and 14 show adjustable speed drive characteristics calculated by the FEM simulation and the mathematical model, respectively. Both of the figures indicate very similar characteristics and the same trends.

TABLE III. LEAKAGE INDUCTANCE COEFFICIENTS.

| | $K_{Ld}$ | $K_{Lq}$ | $K_{d\text{-}axis}$ |
|---|---|---|---|
| 500 r/min | 0.5 | 0.5 | 0.2 |
| 1000 r/min | 0.5 | 0.5 | 0.2 |
| 2000 r/min | 0.4 | 0.5 | 0.2 |
| 3000 r/min | 0.35 | 0.5 | 0.2 |

As discussed in Eq. (19), the higher electromagnet torque is delivered as the synchronous rotation speed increases because the torque generated by the proposed motor is proportional to the speed. The MTPA (Maximum Torque Per Ampere) control angle advances with the increase of the speed. On the other hand, the electromagnet torque generated by the space harmonics is limited by the magnetic saturation of the rotor teeth or the stator teeth.

## V. CONCLUSION

This paper has proposed a novel rare-earth-free motor that can utilize space harmonics power for field magnetization instead of permanent magnets. The operation principle of the proposed motor has been explicated by voltage equations and torque equation on the synchronous rotating reference frame. The comparison of the current phase vs. torque characteristics has been conducted between analyzed results by the FEM model and calculated results by the mathematical model, which verifies feasibility of the mathematical model. The future work is to develop a prototype machine and to examine the various operation characteristics of the machine through experimental tests. Figures 15 to 17 illustrate three-dimensional component exploded views of the prototype. The E-pole windings are mounted on the rotor iron core as shown in Fig. 15 to improve the slot space factor. Both of the E-pole and the I-pole windings are connected with connection boards on the rotor ends as shown in Fig. 17, and the diodes are fixed on the connection boards by using resin mold.

## REFERENCES

[1] M. Azuma, M. Hazeyama, M. Morita, Y. Kuroda, and M. Inoue, "Driving Characteristics of a Claw Pole Motor Using Field Excitation for Hybrid Electric Vehicles," *IEEJ Technical Meeting on Vehicle Technology*, pp. 37-40, 2011 (in Japanese).

[2] Y. Kuwahara, T. Kosaka, N. Matsui, Y. Komada, and H, Kajiura, "Drive Performance Evaluation of Wound Field Flux Switching Motor for HV Drives," *IEEJ Technical Meeting on Vehicle Technology*, VT-13-023, pp. 49-54, 2013 (in Japanese).

[3] S. Nonaka and K. Kesamaru, "Blushless Three-Phase Synchronous Generator without Exciter," *IEEJ Trans. on Industry Applications*, vol. 105, no. 10, pp. 851-858, 1985 (in Japanese).

[4] S. Nonaka, "The Brushless Self-Excited Type Single-Phase Synchronous Generator," *IEEJ Trans.*, vol.82, No.883, pp. 627-634, 1962 (in Japanese).

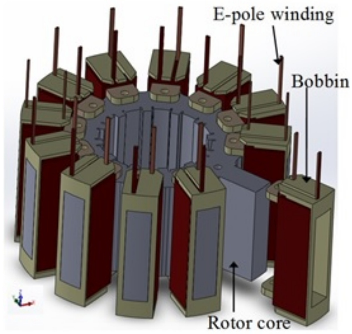


Fig. 15. Mechanical configuration of E-poles.

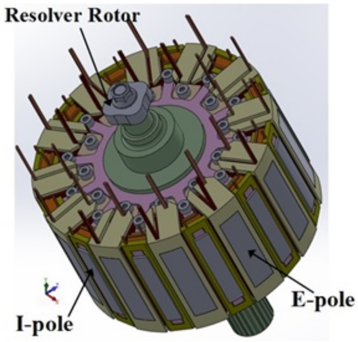


Fig. 16. Rotor assembly without rotor winding connection boards.

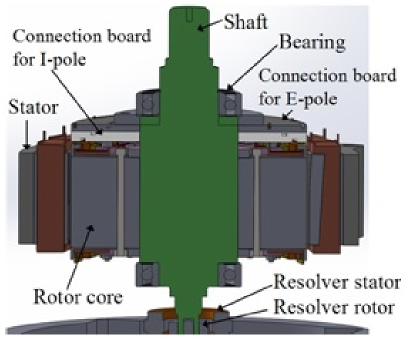


Fig. 17. Vertical cross section diagram of proposed motor.